Lawrence Berkeley National Laboratory

Title

The Beginning of Kinesin's Force-Generating Cycle Visualized at 9 Angstrom Resolution

Permalink

https://escholarship.org/uc/item/0c82b5sc

Authors

Sindelar, Charles V.
Downing, Kenneth H.

Publication Date

2007-06-20

Peer reviewed

The Beginning of Kinesin's Force-Generating Cycle Visualized at 9Å Resolution

Charles V. Sindelar and Kenneth H. Downing*

Life Sciences Division, Lawrence Berkeley National Laboratory, Berkeley, CA 94720

* Author to whom correspondence should be addressed. Email: khdowning@lbl.gov; FAX: 510-486-6488; telephone: 510-486-5941

Abstract

We have used cryo-electron microscopy of kinesin-decorated microtubules to resolve the structure of the motor protein kinesin's crucial nucleotide response elements, switch I and the switch II helix, in kinesin's poorly understood nucleotide-free state. Both of the switch elements undergo conformational change relative to the microtubule-free state. The changes in switch I suggest a role for it in "ejecting" ADP when kinesin initially binds to the microtubule. The switch II helix has an N-terminal extension, apparently stabilized by conserved microtubule contacts, implying a microtubule activation mechanism that could convey the state of the bound nucleotide to kinesin's putative force-delivering element (the "neck linker"). In deriving this structure we have adapted an image processing technique, single-particle reconstruction, for analyzing decorated microtubules. The resulting reconstruction visualizes the asymmetric seam present in native, 13-protofilament microtubules, and this method will provide an avenue to higher-resolution characterization of a variety of microtubule-binding proteins as well as the microtubule itself.

Introduction

Kinesin (Brady, 1985; Vale et al., 1985) is a force-generating molecule that is probably ubiquitous and essential in organisms with microtubules. In neurons, it powers vesicular trafficking directed toward the synapse; in all cells it is involved in the restructuring that occurs during cell division (Kreis and Vale, 1999). This exquisite molecular machine can convert up to 35% of the chemical energy released by ATP hydrolysis into mechanical energy (Nishiyama et al., 2002) as the dimeric form "walks" step-by-step along microtubule protofilaments (Block, 1998). Numerous measurements have characterized kinesin's biophysical properties (Howard, 2001; Peterman et al., 2004).

Atomic resolution structures of monomeric kinesin obtained by X-ray crystallography revealed a "switch I/switch II" nucleotide-sensing architecture, similar to that found in G-proteins and myosins (Kull et al., 1996; Sablin et al., 1996). Moreover, a "relay helix" hypothesis emerged from the crystal structures and other data (Vale and Milligan, 2000). Based on the observation of two distinct conformations of the "switch II helix," crystal structures of kinesin were designated as either "ATP-like," or "ADP-like." In the hypothesis (presented in an adapted form below, as Fig. 5c-d), the switch II helix of ADP-bound and nucleotide-free kinesin (the first two nucleotide states, respectively, of microtubule-bound kinesin) would be positioned away from the nucleotide catalytic site. This conformation of the switch II helix, it was proposed, would resemble that found in the class of kinesin crystal structures regarded as "ADP-like." In ATP-bound kinesin, according to the hypothesis, the switch II helix moves towards the nucleotide active site, mimicking the switch II helix conformation found in a second class of kinesin crystal structures, regarded as "ATP-like." This switch II helix movement was hypothesized to control kinesin's presumed force-delivering element, the "neck linker", by obstructing the neck linker's docking onto the core of kinesin in the "ADP-like" position and permitting docking in the "ATP-like" position.

The first direct tests of the relay helix hypothesis have been incomplete and contradictory. A pair of newly published cryo-electron microscopy (cryo-EM) structures

at a resolution of ~1nm of the KIF1A kinesin (Kikkawa and Hirokawa, 2006) are consistent with the relay helix theory for two of the three principal nucleotide states, finding the switch II helix "ADP-like" in ADP-bound, microtubule-bound kinesin, and "ATP-like" in microtubule-bound kinesin with the non-hydrolyzable ATP analog AMPPNP. However, nucleotide-free kinesin was not included in the KIF1A study. Furthermore, a second very recent cryo-EM study of a different, unconventional kinesin (Kar3) is seemingly at odds with the relay helix theory (Hirose et al., 2006). In Kar3, the switch II helix was visualized apparently in the "ADP-like" position for both the ADP•kinesin•microtubule and AMPPNP•kinesin•microtubule states. Moreover, in the nucleotide-free state of Kar3 the switch II helix was only partially visible, and was interpreted to have restructured as a loop. Thus, the generality of the relay helix theory is in doubt and the role of the nucleotide-free state of kinesin in particular is highly unclear.

Another puzzle related to the relay helix theory concerns the communication between the nucleotide pocket and the switch II helix. Instead of showing clearly defined, nucleotide-dependent states for switch II, the crystal structures showed a range of positions for the switch II helix—apparently unconnected to the identity of the active site nucleotide. For example, it was possible to crystallize KIF1A with an "ATP-like" switch II helix conformation but with ADP in the active site (Kikkawa et al., 2001), in contrast to "ATP-like" switch II helix conformations found in crystal forms reported with either AMPPCP (Kikkawa et al., 2001) or AMPPNP (Nitta et al., 2004). On the other hand, the more recent structures of KIF2C kinesin display an "ADP-like" switch II helix conformation in the presence of either ADP or AMPPNP (Ogawa et al., 2004). Also, EPR and crystallography studies of human KHC kinesin confirmed that in solution kinesin freely exchanges between "ATP-like" and "ADP-like" conformations in the presence of either ADP or AMPPNP (Sindelar et al., 2002). Thus, while microtubule-bound kinesin is hypothesized to have the conformation of its switch II helix controlled by the active site nucleotide, crystallography experiments to date have only identified "uncontrolled" switch II helix movements.

We have previously speculated how microtubule binding may activate kinesin's switch II nucleotide sensing mechanism by structuring kinesin's loop "L11," N-terminally adjacent to the switch II helix (Sindelar et al., 2002). However, other subsequent reports have not addressed this aspect of kinesin's mechanism.

Here we employ a new method of cryo-EM data analysis that, when combined with high-quality image data, can attain better than nanometer-resolution reconstructions of the kinesin-microtubule complex. Our resulting structure of nucleotide-free kinesin complexed to the microtubule exhibits at least three remarkable features. By directly visualizing the switch II helix, we find that the helix is in an "ADP-like" position, confirming one aspect of the relay helix theory for our KHC kinesin construct—in striking contrast to the nucleotide-free Kar3 structure with an apparently "melted" switch II helix. Furthermore, we show that the switch II helix is N-terminally extended by rearrangement of the loop L11 (which is unstructured in crystal structures of our construct). This structured extension, apparently stabilized by microtubule contacts, is a prime candidate for explaining the microtubule-induced activation of kinesin's switch II nucleotide sensing mechanism. Finally, we infer a possible role for switch I in disrupting kinesin's interactions with ADP upon binding to the microtubule.

Results and Discussion

Identifying and Reconstructing the Microtubule Seam

To determine the structure of the asymmetric, 13-protofilament microtubule, we applied "single-particle" reconstruction techniques (see Methods) to our set of nucleotide-free kinesin-decorated microtubule images. The essential step of the single-particle analysis was to determine the orientation of a given microtubule's symmetry-disrupting "seam." Once the seam orientations were identified in our imaged, kinesin-decorated microtubules, we produced a 15Å-resolution reconstruction of the entire, asymmetric microtubule volume (see Methods). The reconstruction, shown in Fig. 1, clearly reveals the microtubule seam, validating our reconstruction techniques. Seams in microtubules have been imaged before (Kikkawa et al., 1994; Sosa et al., 1997), but 3D reconstructions have never been produced of the native 13-protofilament form, because of technical limitations in image processing. Here we have applied a method capable of reconstructing the 13-protofilament microtubule form, and have derived a cryo-EM reconstruction of this form including the asymmetric seam.

A High-Resolution Kinesin-Microtubule Complex Structure

To maximize the resolution of the nucleotide-free kinesin-microtubule complex, we averaged together the 13 unique protofilaments reconstructed in Fig. 1 to produce a new motor-tubulin complex with the highest possible signal-to-noise ratio. After this step and subsequent image processing (see Methods), we derived the kinesin-tubulin complex shown in Figs. 2-4. We note that in the averaging step, we assumed that all 13 copies of the motor-tubulin complex were identical—an assumption that could in principle be violated since our structure contained an asymmetric seam. However, inspection of our non-averaged reconstruction (Fig. 1) does not reveal obvious conformational differences between different sites (for example, differing motor occupancy or orientation), justifying our assumption at least to the first approximation.

At the resolution of the symmetry-averaged structure, about 9Å (see Methods), helices in tubulin were distinct from one another, even the packed antiparallel helices H11 and H12 (Fig. 2a). All helices in kinesin were resolved but were slightly less distinct, possibly due to imperfect occupancy (estimated to be about 75%) on the microtubule lattice. However, the large beta sheet at the core of kinesin appeared as a continuous twisted sheet of density, a loop (L8 in kinesin) appeared as a distinct arm connecting kinesin to the microtubule surface, and the switch II helix was clearly resolved at the microtubule binding interface.

To evaluate tubulin's secondary structure elements, the coordinates of bovine tubulin (PDB ID 1JFF (Lowe et al., 2001)) were fitted into the cryo-EM map using cross-correlation implemented in Fourier space with the COLORES program from the SITUS package (Wriggers and Birmanns, 2001). The agreement between positions of helices in our map and the fitted tubulin crystal structure was excellent (Fig. 2a and Supplemental Movie 1).

The Switch II Helix is "ADP-like"

Two crystal structures of monomeric human kinesin, those of the K349 construct (used in our experiments) with and without a docked neck linker (PDB ID's 1MKJ (Sindelar et al., 2002) and 1BG2 (Kull et al., 1996), respectively), were fit into our map using COLORES, as above. The positioning of the molecules was unambiguous, with alignments between the two fitted core motor domains differing by less than 2°, when the principal axes of the moments of inertia were compared using the program GEM (Browner et al., 1992). The fit of the crystal structure into our molecular envelope is excellent in most regions of the protein chain (Fig. 2b and Supplemental Movie 2). However, the docked neck linker present in 1MKJ was found to be out of density (Fig. 2c). No compensating region of unoccupied density was found near the docked neck linker region. Thus, our density map strongly suggests that the neck linker is disordered in our experimental conditions. This result agrees with numerous other experiments

employing techniques including single molecule fluorescence (using bifunctional labels) (Asenjo et al., 2006) and EPR (Rice et al., 1999).

In all crystal structures observed to date, a disordered neck linker in kinesin is accompanied by a switch II helix in the "ADP-like" position; furthermore, the switch II helix in the ADP•kinesin•microtubule complex (with a disordered neck linker) was likewise in the "ADP-like" position (Kikkawa and Hirokawa, 2006). It therefore seemed likely that the nucleotide-free kinesin•microtubule complex would have an "ADP-like" switch II helix conformation as well (Vale and Milligan, 2000). Our cryo-EM map allowed this prediction to be tested directly, because density corresponding to the switch II helix was clearly apparent.

We compared the position and orientation of the density corresponding to the switch II helix in our map with the switch II helix positions predicted by crystal structure fits, using ~20 kinesin crystal structures from the PDB. As shown in Fig. 3a-b, our helical density falls within the switch II helix orientations classified as "ADP-like" from K349 and KIF1A crystal structures as well as others (not shown). We quantified this observation by fitting a long switch II helix from Kar3 (not shown, but see Fig. 3c below) into our density using SITUS, and comparing the principal axis of the moment of inertia of this fitted helix (calculated by GEM) with the principal axes of the K349 and KIF1A helices. This analysis showed that the KIF1A "ADP-like" switch II helix was rotated approximately 8° counterclockwise (in the plane of the Figure) compared to our helical density, while the K349 "ADP-like" helix was rotated approximately 6° clockwise. Thus, "ADP-like" switch II helices can vary over a significant range of orientations relative to the core motor domain, and our switch II helix density lies squarely in this range.

On the other hand, fitted kinesin structures with switch II helices having "ATP-like" conformations were distinct from our helix density, as shown in Fig. 3b. In particular, the C-termini of the crystal structure helices (on the right-hand side of the Figure) are well out of density and far from the apparent helical axis of the density. A moment of

inertia comparison showed the "ATP-like" switch II helices to be rotated ~12-15° clockwise in the plane of the Figure, relative to the helix density. This angular difference, significantly greater than the estimated error of our orientation determination (~5°), demonstrates that the switch II helix orientation in our structure is measurably distinct from that found in the "ATP-like" crystal structures. Taken together, these results constitute direct evidence to support the "relay helix" prediction of kinesin's switch II helix "ADP-like" conformation in the nucleotide free, microtubule-bound state.

A Microtubule-Stabilized Extension of the Switch II Helix

A significant N-terminal extension of the switch II helix, relative to the crystal structures of our K349 construct, is evident in our cryo-EM density map in Fig. 3. The visible density extends the helix by several turns. Furthermore, the extension in our map is accompanied by an extra "sphere" of density, closely associated with the microtubule surface, in the vicinity of the N-terminus of the helix. Intriguingly, these features correspond to the architecture of switch II seen in several crystal structures (Kikkawa et al., 2001; Nitta et al., 2004; Shipley et al., 2004), including that of Kar3 (mutation R598A) (Yun et al., 2001), as shown in Fig. 3c. The structural element at the N-terminus of the switch II helix, loop L11, is often disordered in crystal structures but visible in that of Kar3, and projects through the "sphere" of density in our alignment.

The structural alignment in Fig. 3c serves as a useful indicator of residues likely to be involved in the kinesin-microtubule interaction for kinesin's nucleotide free state. This alignment indicates that the two space-filled residues shown in Fig. 3c (corresponding to Asn 255 on the K349 switch II helix and Thr 241 on K349 loop L11), highly conserved in the kinesin family (Sablin et al., 1996), account for the two microtubule contact points of the switch II helix extension-L11 assembly. Both of these residues are involved in the microtubule-induced restructuring of kinesin seen in our cryo-EM structure. In the fitted ADP-like K349 crystal structure in Fig. 3a, not only does the sidechain of Asn 255 face away from the microtubule surface (not shown), but also the backbone departs from the alpha-helical structure of subsequent residues 256-271 of the switch II helix. In contrast,

the equivalent residue Asn 650 contained within the alpha-helical extension of Kar3 (Fig. 3c) has swiveled ~180° to point its sidechain at microtubule helix H11' and/or the subsequent loop on the microtubule surface.   Residue Thr 241 is not present in the K349 crystal structure and is presumably disordered, while the equivalent residue Ser 636 in the Kar3 model faces helix H3' on the microtubule surface. Thus, our modeling suggests that rearrangement of critical conserved microtubule-binding residues in kinesin supports the restructuring of switch II and L11 seen in our nucleotide-free kinesin•microtubule complex.

ADP Release Does Not Strongly Reorient Kinesin on the Microtubule

We compared the microtubule-bound orientation of our fitted K349 core domain with that of ADP-bound and AMPPNP-bound KIF1A reported by Kikkawa and Hirokawa (Kikkawa and Hirokawa, 2006) (PDB ID's 2HXF and 2HXH). A least-squares superposition and moment-of-inertia analysis by the GEM program showed only a 5° rotation of the core domain of our structure compared to ADP-bound KIF1A. On the other hand, AMPPNP-bound KIF1A was reoriented by 15° relative to our structure. Thus, our nucleotide-free K349 core domain orientation is much more similar to ADP-bound, microtubule-complexed KIF1A.   Since kinesin's orientation on the microtubule is hypothesized to depend on whether the switch II helix is "ATP-like" or "ADP-like", the similarity between our structure and ADP-bound KIF1A is further confirmation that the switch II helix is "ADP-like" in both structures.

Restructuring of the Nucleotide Pocket

To compare the nucleotide pocket in our experimental map with that expected from crystal structures of K349•ADP, we generated a 9Å-resolution synthetic map using the fitted PDB coordinates of "ADP-like" K349 (but with ADP omitted) and tubulin from Fig. 2b, above.   At this resolution, several structured loops are visible as lobes of density in both synthetic and experimental maps. Examples include kinesin's loops L5 and L8 (see Figs. 2 and 4), as well as the loop between tubulin's beta strands B9 and B10 (not

shown). This observation suggests it is feasible to detect, in our maps, conformational change of kinesin's nucleotide binding pocket, which contains two functionally significant loops: the ADP-coordinating "P-loop," and the Switch I nucleotide response element.

When viewed at an isocontour level of ~2 σ, as shown in Fig. 4a-b, the synthetic map displays a lobe of density marking the location of the P-loop. In the experimental density map, however, this lobe does not appear even at lower contour levels (Fig. 4b, d). This difference, which was consistently observed in reconstructions using two independent half data sets (not shown), suggests a rearrangement of the P-loop in kinesin's nucleotide-free state relative to crystal structures.

While no alternative density site for the P-loop is apparent at the 2 σ contour level in our map of nucleotide-free kinesin, at a lower threshold (1.2 σ) a "bridge" is revealed in our experimental map between the density for switch I and the P-loop site, as shown in Fig. 4d. The bridge, which features a distinctive protuberance, was consistently observed in two independent half data set reconstructions (Fig. S3). The appearance of this bridge is accompanied by a rotation and shortening of helix α3, N-terminal to the switch I loop, and a movement of the switch I density itself towards the nucleotide site as it forms the bridge (Fig. 4d).

These observations suggest a model for ADP release by kinesin following microtubule binding (Hackney, 1988). In guanine nucleotide-binding proteins, whose mechanism of nucleotide release is somewhat better understood, a consistent feature of the nucleotide-free state is disruption of the P-loop— evidently contributing to nucleotide release (Vetter and Wittinghofer, 2001). This disruption appears to be caused by any of a variety of mechanisms, including direct interactions between the P-loop and residues of the guanine-nucleotide exchange factor (GEF), or an indirect pathway such as GEF-modulated conformational change of switch II that in turn disrupts the P-loop. As shown in Fig. 4d, our data are consistent with a disruption of the P-loop, but suggest that interactions by switch I may contribute to the disruption.

A probable trigger for the apparent restructuring of switch I in our structure is the microtubule-induced restructuring of L11 and the N-terminal extension of switch II as described above (Fig. 3). As seen in Fig. 4b, switch I in our structure approaches the extended switch II N-terminus, possibly attracted by new contacts made available by the L11/switch II restructuring. Indeed, based on the Kar3 model of Fig. 3c, absolutely conserved residue Glu 250 in the switch II helix extension would be positioned at the interface where our density for switch I meets the helical extension (not shown). Furthermore, in a KIF1A "ADP-like" crystal structure—with an extended switch II helix— the equivalent of K349's Glu 250 forms a salt bridge with the equivalent of K349's Arg 203 from switch I. Thus, given the proximity between the switch II helix and switch I in our structure, it is likely that this conserved interaction forms there as well.

This potential chain of communication, from switch II to switch I to the nucleotide pocket, is supported by experiments that showed that mutations in either switch I (equivalent to R203A in our K349 construct) or switch II (equivalent to N255K or E236A in K349) decoupled microtubule binding from kinesin's ADP affinity (Yun et al., 2001). Our structure suggests a more detailed explanation for the decoupling mechanism, particularly in the case of the Asn mutation. If the N255K mutation destabilizes the helical extension by changing the residue's microtubule interactions, then in our mechanism the extension would no longer be present to attract switch I towards the nucleotide site while kinesin is bound to the microtubule. Thus, microtubule binding would no longer eject ADP and would be uncoupled from ADP affinity.

Mechanism of Plus—End Directed Motors Appears Distinct from that of Kar3

Taken together with the ADP and AMPPNP kinesin-microtubule complexes of (Kikkawa and Hirokawa, 2006), our nucleotide-free structure completes a nanometer-resolution picture of the nucleotide binding and hydrolysis cycle for the "plus end-directed"

kinesins. Notably, the position of the switch II helix was identified for all three of these nucleotide states and in each case was found to agree with the predictions of the relay helix theory.

It is significant that structures of Kar3 complexed to the microtubule (Hirose et al., 2006) do not appear to follow the relay helix paradigm, as mentioned in the Introduction. While it is hard to reconcile these results with ours and those of (Kikkawa and Hirokawa, 2006), we note that Kar3 moves towards the minus end of the microtubule, while our KHC construct and KIFA are a plus-end directed motors. As such, Kar3 possesses a different force-delivering element, the helical "neck" (Sablin et al., 1998) (as opposed to conventional kinesin's neck linker). Thus, it is at least conceivable that minus-end-directed kinesins have evolved a switch II mechanism distinct from the "relay helix."

Model for Microtubule Activation of the Relay Helix

The mechanism that communicates the state of the nucleotide to the switch II helix is a crucial, unknown component of the proposed relay helix mechanism for kinesin. This mechanism presumably involves the formation of a hydrogen bond between switch II's absolutely conserved Gly 234 and ATP's gamma phosphate—a critical feature conserved as far as is known across proteins with functional switch II domains (Sablin and Fletterick, 2001). One possibility for this mechanism is our "connecter" hypothesis, depicted in Fig. 5c-d.

We predict that this "connecter," consisting of our observed N-terminal extension of the switch II helix as well as the C-terminal, microtubule-contacting segment of L11, forms upon microtubule binding and persists after ATP binds in kinesin's active site (Fig. 5d). In this process the microtubule contacts would act as a kind of "glue," stabilizing the connecter so that ATP-induced movement of Gly234 and the adjacent, N-terminal segment of L11 would be transmitted through the relay helix to the neck linker. The apparent microtubule interactions of conserved residues Thr 241 and Asn 255 in our structure, sufficient to stabilize and restructure a portion of L11 relative to crystal

structures, reinforce this idea. The fact that some crystal structures of kinesin show N-terminal extensions of the switch II helix relative to our construct show that such an extension is possible, if not necessarily stable in the absence of microtubules. Furthermore, density consistent with the helical extension is evident in both ADP- and AMPPNP-bound forms of the KIF1A•microtubule complex (Kikkawa and Hirokawa, 2006).

Though an N-terminal extension of the switch II helix is not seen in the AMPPNP•KIF1A crystal structure (Nitta et al., 2004), it is unlikely in any case that the conformations of L11 and the adjoining Gly 234 are the same in the ATP•kinesin•microtubule complex as in the crystal structure. This is because the AMPPNP•KIF1A crystal structure lacks a hydrogen bond between the nucleotide's gamma phosphate and KIF1A's Gly 251 (the equivalent of Gly 234 in K349). The switch II helix extension we propose in the ATP state of the kinesin-microtubule complex could help lead to the formation of such a hydrogen bond. Further work to extend the resolution of the kinesin-microtubule complex will be required to fully elaborate the role of L11 and Gly 234 in kinesin's ATP-sensing mechanism.

Summary

Our structure has allowed us to propose further details of how microtubule binding affects kinesin's interactions with bound nucleotide—in particular, how it may release bound nucleotide upon microtubule binding and how microtubule binding may permit the switch II helix to respond to the identity of kinesin's active-site nucleotide. Furthermore, our structure determination methods open up a route to high-resolution characterization of lateral interactions of the microtubule protofilaments—even those that occur at the microtubule seam. Future work will extend the resolution of both kinesin and the microtubule, allowing us to test the various aspects of the structural mechanisms of these proteins.

Materials and Methods

Sample Preparation

Human monomeric kinesin K349 cys-lite, derived from the conventional human kinesin heavy chain (KHC), was prepared as described (Rice et al., 1999). We chose the mutant form 220C, which has motility and hydrolysis properties close to wild-type kinesin (Rice et al., 1999), for its high purification yield (~100mg per 2L culture). After elution from the final column (mono Q), ~1mL aliquots of roughly 2mg/mL were frozen in elution buffer + 20% sucrose. For use in EM experiments, protein was thawed on ice and dialyzed overnight against binding buffer (25mM PIPES pH 6.8, 25mM NaCl, 1mM EGTA, 2mM $MgCl_2$). The resulting protein solution was concentrated to 15-20 mg/mL using centricon concentrators (Millipore). After this treatment our kinesin preparation remained stable with significant microtubule binding activity after several months at +4 degrees C, making it an especially useful construct for extended experimental study.

Glycerol-free tubulin was purchased from Cytoskeleton, Inc. (Denver, CO) and polymerized according to a modified protocol to minimize aggregated, nonpolymerized tubulin. Frozen tubulin aliquots (25 µL) were thawed on ice and ultracentrifuged at maximum speed for 10 minutes (100K RPM, Beckman TLA 120.2 rotor). The supernatant was added to a chilled glass vial, 1mM GTP was added, and the vial placed in a 37-degree incubator for 15 minutes. At this point 1.25 µL of taxol (2mM in DMSO), diluted in 11.25 µL of polymerization buffer (PEM -- 80mM PIPES pH 6.8, 1mM EGTA, 2mM $MgCl_2$), was slowly and carefully stirred into the polymerization vial. After 15-30 more minutes 12.5 µL of the polymerized microtubules were mixed with ~25 µL of above-prepared kinesin solution and 5 µL of apyrase (10 mg/mL in deionized water). After 5 minutes this mixture was layered onto a room-temperature glycerol cushion (50% glycerol + binding buffer + 200 µM taxol) and ultracentrifuged at 40K RPM for 20 minutes. The resulting kinesin-microtubule pellet was briefly washed 2x with binding buffer + 200 µM taxol and resuspended in 15 µL of the same buffer.

To maintain the kinesin decoration on the microtubules during grid preparation for cryo-EM proved to be extremely difficult. Any of three factors apparently caused the kinesin to dissociate before the grids could be frozen. These factors were (1) glow-discharging the grids; (2) the presence of undiluted salts and buffer molecules from the binding buffer; and (3) blotting for more than a fraction of a second. To overcome these difficulties, we arrived at the following protocol: 0.3 µL of the kinesin-microtubule mixture was added to 3 µL of deionized water and mixed by pipetting. The resulting mixture was applied to a homemade holey carbon grid, and then excess fluid was wicked away by touching the edge of the grid to a piece of filter paper repeatedly-- until the meniscus was barely visible. The grid was then blotted and quickly (<0.5 second later) plunged into liquid ethane. Because our grids were not subjected to glow discharge, the ice was of poor quality and each grid contained relatively few areas suitable for imaging.

Electron Microscopy

Images (~350) were collected on film using a JEOL 4000 microscope operating at 400kV and 60kx magnification, with defocus values ranging from 0.8 microns to 2 microns. Developed films were scanned using a robotic system incorporating a Nikon CoolPix Scanner operating at 6.3 micron/pixel (Typke et al., 2005). The final digitized images had a sampling of ~1Å per pixel.

Single-Particle Image Analysis

Thirteen-protofilament microtubules were selected manually using the boxer program of the EMAN package (Ludtke et al., 1999), whose interactive functions facilitated the division of each microtubule into short (750 x 750-pixel) overlapping segments. Subsequent single-particle image processing was carried out using customized scripts written for the SPIDER package (Frank et al., 1996), and roughly followed the methodology described by (Li et al., 2002).

To generate an initial model for reference-based alignment, the atomic microtubule model of (Li et al., 2002) was "decorated" using the crystal structure of human monomeric kinesin in orientations reflecting the AMPPNP-bound kinesin-microtubule complex of (Kikkawa et al., 2001). Reference projections of this volume (filtered to ~1nm resolution) were then calculated at 0.3° intervals around the microtubule axis including up to +/- 25° out-of-plane tilt. While we did not expect our final map to exactly resemble this initial atomic model, the (significant) differences between our final map and the initial reference model served as a control to ensure that our reconstruction methods were not simply reproducing the model with which we started.

Finding the Seam

Reference-based analysis of kinesin-decorated 13-protofilament microtubules (Figs. S1-S2) was complicated by the presence of a "seam" that disrupts the quasi-helical symmetry (Mandelkow et al., 1986). The practical implication of the seam was that a complete 360-degree axial rotation of the decorated reference microtubule produced 13 fairly close "matches" against an experimentally imaged microtubule segment-- of which only one gave the correct seam alignment. However, small but significant differences in the magnitude of the image-reference cross-correlation indicated the true position of the seam (Fig. S2). Furthermore, seam determinations along consecutive microtubule segments typically agreed, amplifying our certainty that we had correctly identified the seam position. The low signal-to-noise ratio in our images caused a significant fraction (frequently 25% or more) of boxed segments to yield incorrect seam identifications that were one or more protofilaments away from the "correct" seam identified by the majority of segments. However, this type of error decreased when increasingly accurate reference models were used in subsequent rounds of refinement.

Occasional microtubules produced extremely poor seam alignments, which appeared to jump randomly or cyclically between seam orientations with each segment. We identified these microtubules as 12- or 14-protofilament ones that had eluded the initial

visual screening process. Thus, our reference alignment procedure also served as a backup screen for 13-protofilament microtubules.

3D Volume Reconstruction

After reference-based alignments were derived for the microtubule segments (see Figs. S1-S2), a 3D volume was obtained by weighted back-projection. To increase the quality of our final map, the back projection process was modified to directly integrate contrast transfer function (CTF) correction via a customized C program. The goal of the modification was to implement CTF correction with CTF-squared weighting of the Fourier components of the images, resembling helical reconstruction methods presented, for example, by (Yonekura and Toyoshima, 2000). Within the program, the Fourier transform of each microtubule segment was first multiplied by its experimentally determined CTF (which included astigmatism). The CTF was derived by straightening entire microtubules using previously determined reference alignment parameters; the entire microtubule was then Fourier transformed to find the position and shape of the layer line absences indicating CTF minima. Subsequently in the program (but before back-projection) the Fourier transform of each image was multiplied by a general, exponential weighting function derived from all other image segment transforms overlapping in Fourier space (Frank et al., 1996), and divided by the sum of the squares of the CTFs for the overlapping Fourier space measurements. The general exponential weighting function used was identical to that employed in SPIDER's "bp 3d" command. The resulting Fourier space object was inverse-Fourier-transformed into an image and back-projected through the target volume; this process was repeated for all microtubule segments to produce a final volume

Another feature of our volume reconstruction methods took advantage of the pseudo-symmetry of the 13-protofilament microtubules used here. As mentioned above, the seam disrupted true helical symmetry in the microtubules. However, it was possible to average the 13 pseudo-symmetry-mates in Fourier space, during back projection, to improve the resolution of the basic kinesin-tubulin subunit along one protofilament. The most

straightforward way to describe our symmetry averaging method is to describe the real-space analog. Rotating a microtubule volume by $n * 360°/13$ and translating by $n/13$ of the pseudo-helical repeat distance of 12nm (where n is an integer) results in a new volume that superimposes on the original volume except for superimposing alpha tubulin on beta tubulin in n of the protofilaments. Applying this process for $n=0$ to 12 and superimposing the 13 resultant volumes will reveal one protofilament where kinesin and alpha and beta tubulin superimpose for all 13 volumes. Thus, averaging the 13 volumes produced this way results in a strange volume that has one correctly averaged protofilament. To apply this idea in Fourier space before back projection, we created 13 copies of each segment image, corresponding to $n=0$ to 12. We then added $n * 360/13$ to the reference-determined axial orientation parameter of segment, and translated the segment in the axial direction of the microtubule by $n/13$ of the repeat distance of 12nm. Thus, the input to our back-projection algorithm consisted not only of the original segment images, but also 12 additional copies related by symmetry.

The final volume incorporated data from 131 micrographs, representing 188 microtubules for a total of 2460 unique image segments. Each image segment contained ~9 tubulin dimer repeats multiplied by 13 protofilaments. However, each image segment also overlapped neighboring image segments by ~50%. Thus our reconstruction contained information from 2460 x 9 x 13 x 0.5 tubulin dimer repeats = ~150,000 tubulin dimers.

After the first round of refinement, the reconstructed microtubule volume was filtered to 1.6nm resolution and used to generate a new set of reference images. The reference alignment process was then repeated with the new reference set. The second reference alignment did not change most of the initially discovered orientation parameters by more than 1 degree when compared to the first reference alignment. This agreement indicated that our initial reference model, though it represented the wrong nucleotide state of kinesin, was sufficient to yield relatively high quality orientation parameters in the initial reference alignment.

To compensate for amplitude attenuation at higher resolutions, the reconstruction was sharpened by applying a B-factor of –100, which was derived by comparing resolution-dependent amplitudes of our map to a synthetic map generated from PDB coordinates. The resolution of our reconstructions was estimated by two independent methods. First, the program RMEASURE (Sousa and Grigorieff, 2007) reported a resolution of 15.0Å for the asymmetric reconstruction, and 9.0Å for the symmetry-averaged reconstruction (using the program's conservative output, with an estimated Fourier shell correlation cutoff of 0.5). Second, the Fourier shell correlation (van Heel, 1986) (FSC) was compared between two reconstructions: one using odd- numbered image segments, and the other using even- numbered image segments. The resulting curve descended below FSC=0.5 at 15.1Å resolution for the asymmetric reconstruction, and at 9.1Å resolution for the symmetry-averaged reconstruction.

Public Data Deposition

The coordinates of kinesin and tubulin, fitted into our density map, are available online from the Protein Data Bank(www.rcsb.org) (ID# 2P4N). The density map has been deposited in the EMDB and is available online at http://www.ebi.ac.uk/msd-srv/emsearch/index.html (accession code 1340).

Online Supplemental Material

Figs. S1-S2 illustrate details of the single-particle analysis and 3D reconstruction procedures. Fig. S3 shows two independent half data set reconstructions of kinesin's nucleotide pocket. Videos 1 and 2 are 3D reconstructions of tubulin and kinesin (respectively) from our density map, with superimposed ribbon diagrams of fitted PDB structures.

Acknowledgements

Abbreviations List

AMPPNP, 5'-adenylyl-imidodiphosphate; cryo-EM, cryo-electron microscopy.

References

Asenjo, A.B., Y. Weinberg, and H. Sosa. 2006. Nucleotide binding and hydrolysis induces a disorder-order transition in the kinesin neck-linker region. *Nat Struct Mol Biol*. 13:648-54.

Block, S.M. 1998. Leading the procession: new insights into kinesin motors. *J Cell Biol*. 140:1281-4.

Brady, S.T. 1985. A novel brain ATPase with properties expected for the fast axonal transport motor. *Nature*. 317:73-5.

Browner, M.F., E.B. Fauman, and R.J. Fletterick. 1992. Tracking conformational states in allosteric transitions of phosphorylase. *Biochemistry*. 31:11297-304.

Frank, J., M. Radermacher, P. Penczek, J. Zhu, Y. Li, M. Ladjadj, and A. Leith. 1996. SPIDER and WEB: processing and visualization of images in 3D electron microscopy and related fields. *J Struct Biol*. 116:190-9.

Hackney, D.D. 1988. Kinesin ATPase: rate-limiting ADP release. *Proc Natl Acad Sci U S A*. 85:6314-8.

Hirose, K., E. Akimaru, T. Akiba, S.A. Endow, and L.A. Amos. 2006. Large conformational changes in a Kinesin motor catalyzed by interaction with microtubules. *Mol Cell*. 23:913-23.

Howard, J. 2001. Mechanics of Motor Proteins and the Cytoskeleton. Sinauer, Sunderland, MA. 367 pp.

Kikkawa, M., and N. Hirokawa. 2006. High-resolution cryo-EM maps show the nucleotide binding pocket of KIF1A in open and closed conformations. *Embo J*.

Kikkawa, M., T. Ishikawa, T. Nakata, T. Wakabayashi, and N. Hirokawa. 1994. Direct visualization of the microtubule lattice seam both in vitro and in vivo. *J Cell Biol*. 127:1965-71.

Kikkawa, M., E.P. Sablin, Y. Okada, H. Yajima, R.J. Fletterick, and N. Hirokawa. 2001. Switch-based mechanism of kinesin motors. *Nature*. 411:439-45.

Kreis, T., and R. Vale. 1999. Guidebook to the Cytoskeletal and Motor Proteins. Oxford University Press, New York.

Kull, F.J., E.P. Sablin, R. Lau, R.J. Fletterick, and R.D. Vale. 1996. Crystal structure of the kinesin motor domain reveals a structural similarity to myosin. *Nature*. 380:550-5.

Li, H., D.J. DeRosier, W.V. Nicholson, E. Nogales, and K.H. Downing. 2002. Microtubule structure at 8 A resolution. *Structure*. 10:1317-28.

Lowe, J., H. Li, K.H. Downing, and E. Nogales. 2001. Refined structure of alpha beta-tubulin at 3.5 A resolution. *J Mol Biol*. 313:1045-57.

Ludtke, S.J., P.R. Baldwin, and W. Chiu. 1999. EMAN: semiautomated software for high-resolution single-particle reconstructions. *J Struct Biol*. 128:82-97.

Mandelkow, E.M., R. Schultheiss, R. Rapp, M. Muller, and E. Mandelkow. 1986. On the surface lattice of microtubules: helix starts, protofilament number, seam, and handedness. *J Cell Biol*. 102:1067-73.

Minehardt, T.J., R. Cooke, E. Pate, and P.A. Kollman. 2001. Molecular dynamics study of the energetic, mechanistic, and structural implications of a closed phosphate tube in ncd. *Biophys J*. 80:1151-68.

Nishiyama, M., H. Higuchi, and T. Yanagida. 2002. Chemomechanical coupling of the forward and backward steps of single kinesin molecules. *Nat Cell Biol*. 4:790-7.

Nitta, R., M. Kikkawa, Y. Okada, and N. Hirokawa. 2004. KIF1A alternately uses two loops to bind microtubules. *Science*. 305:678-83.

Ogawa, T., R. Nitta, Y. Okada, and N. Hirokawa. 2004. A common mechanism for microtubule destabilizers-M type kinesins stabilize curling of the protofilament using the class-specific neck and loops. *Cell*. 116:591-602.

Peterman, E.J., H. Sosa, and W.E. Moerner. 2004. Single-molecule fluorescence spectroscopy and microscopy of biomolecular motors. *Annu Rev Phys Chem*. 55:79-96.

Pettersen, E.F., T.D. Goddard, C.C. Huang, G.S. Couch, D.M. Greenblatt, E.C. Meng, and T.E. Ferrin. 2004. UCSF Chimera--a visualization system for exploratory research and analysis. *J Comput Chem*. 25:1605-12.

Rice, S., A.W. Lin, D. Safer, C.L. Hart, N. Naber, B.O. Carragher, S.M. Cain, E. Pechatnikova, E.M. Wilson-Kubalek, M. Whittaker, E. Pate, R. Cooke, E.W. Taylor, R.A. Milligan, and R.D. Vale. 1999. A structural change in the kinesin motor protein that drives motility. *Nature*. 402:778-84.

Sablin, E.P., R.B. Case, S.C. Dai, C.L. Hart, A. Ruby, R.D. Vale, and R.J. Fletterick. 1998. Direction determination in the minus-end-directed kinesin motor ncd. *Nature*. 395:813-6.

Sablin, E.P., and R.J. Fletterick. 2001. Nucleotide switches in molecular motors: structural analysis of kinesins and myosins. *Curr Opin Struct Biol*. 11:716-24.

Sablin, E.P., F.J. Kull, R. Cooke, R.D. Vale, and R.J. Fletterick. 1996. Crystal structure of the motor domain of the kinesin-related motor ncd. *Nature*. 380:555-9.

Shipley, K., M. Hekmat-Nejad, J. Turner, C. Moores, R. Anderson, R. Milligan, R. Sakowicz, and R. Fletterick. 2004. Structure of a kinesin microtubule depolymerization machine. *Embo J*. 23:1422-32.

Sindelar, C.V., M.J. Budny, S. Rice, N. Naber, R. Fletterick, and R. Cooke. 2002. Two conformations in the human kinesin power stroke defined by X-ray crystallography and EPR spectroscopy. *Nat Struct Biol*. 9:844-8.

Sosa, H., A. Hoenger, and R.A. Milligan. 1997. Three different approaches for calculating the three-dimensional structure of microtubules decorated with kinesin motor domains. *J Struct Biol*. 118:149-58.

Sousa, D., and N. Grigorieff. 2007. Ab initio resolution measurement for single particle structures. *J Struct Biol*. 157:201-10.

Typke, D., R.A. Nordmeyer, A. Jones, J. Lee, A. Avila-Sakar, K.H. Downing, and R.M. Glaeser. 2005. High-throughput film-densitometry: an efficient approach to generate large data sets. *J Struct Biol*. 149:17-29.

Vale, R.D., and R.A. Milligan. 2000. The way things move: looking under the hood of molecular motor proteins. *Science*. 288:88-95.

Vale, R.D., T.S. Reese, and M.P. Sheetz. 1985. Identification of a novel force-generating protein, kinesin, involved in microtubule-based motility. *Cell*. 42:39-50.

van Heel, M. 1986. Similarity measures between images. *Ultramicroscopy*. 21:95-100.

Vetter, I.R., and A. Wittinghofer. 2001. The guanine nucleotide-binding switch in three dimensions. *Science*. 294:1299-304.

Wriggers, W., and S. Birmanns. 2001. Using situs for flexible and rigid-body fitting of multiresolution single-molecule data. *J Struct Biol*. 133:193-202.

Yonekura, K., and C. Toyoshima. 2000. Structure determination of tubular crystals of membrane proteins. III. Solvent flattening. *Ultramicroscopy*. 84:29-45.

Yun, M., X. Zhang, C.G. Park, H.W. Park, and S.A. Endow. 2001. A structural pathway for activation of the kinesin motor ATPase. *Embo J*. 20:2611-8.
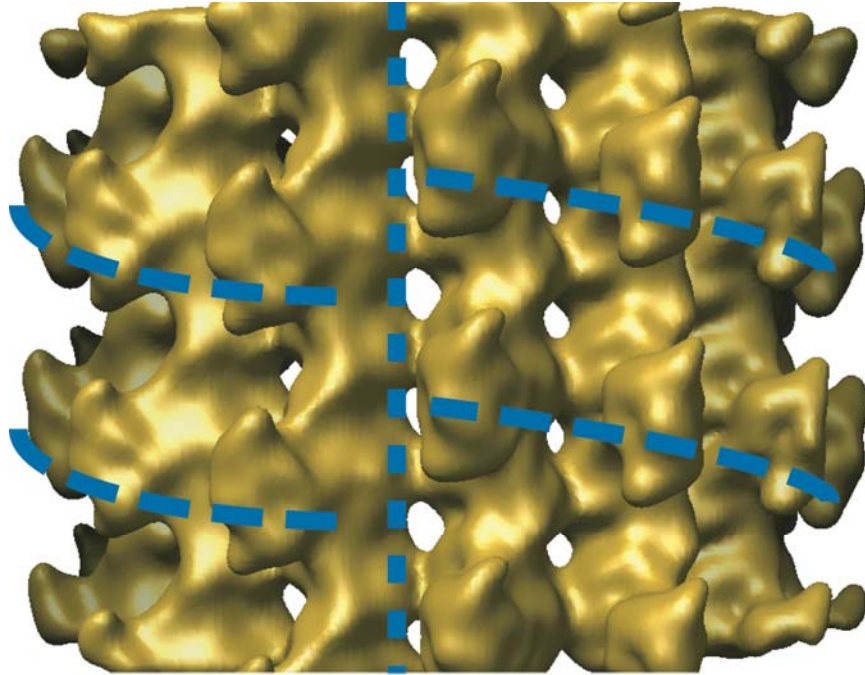
Figure Legends

Figure 1

Figure 1. Isosurface view of the reconstruction of the microtubule seam. Note that this reconstruction is filtered to a resolution of 15Å and, unlike the symmetry-averaged one presented in the following Figures, is not amplitude-sharpened. The vertical dashed line indicates the location of the seam; horizontal curved dashed lines indicate the helical path of the bound kinesin monomers, interrupted by the seam.
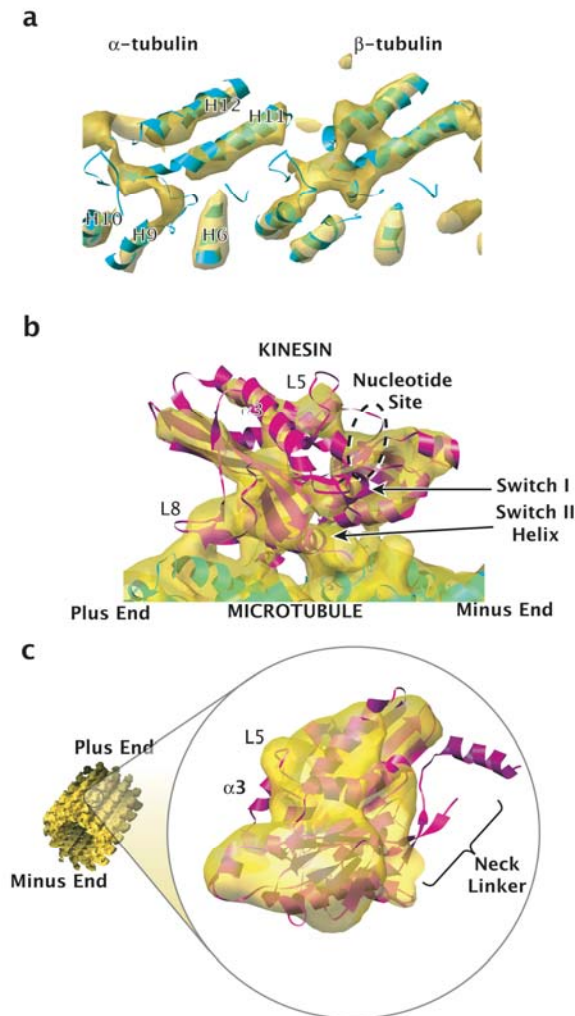
Figure 2

Figure 2. Fits of the K349 kinesin crystal structures into our cryo-EM map, suggesting a disordered neck linker. (a) Representative density in the microtubule region of our cryo-EM map (gold), and the fitted crystal structure of tubulin (blue). See Video 1. Molecules and surfaces rendered with UCSF Chimera (Pettersen et al., 2004).

 (b) Fit of the "ADP-like" K349 crystal structure (Kull et al., 1996) into the map, indicating the location of various structural elements (Video 2). (c) Fit of the "ATP-like" K349 crystal structure (Sindelar et al., 2002) into the map, demonstrating that the neck linker is out of density. The C-terminus of kinesin's helix α3 is also out of density, possibly correlated to a rearrangement of Switch I (see Figure 7 and accompanying text).
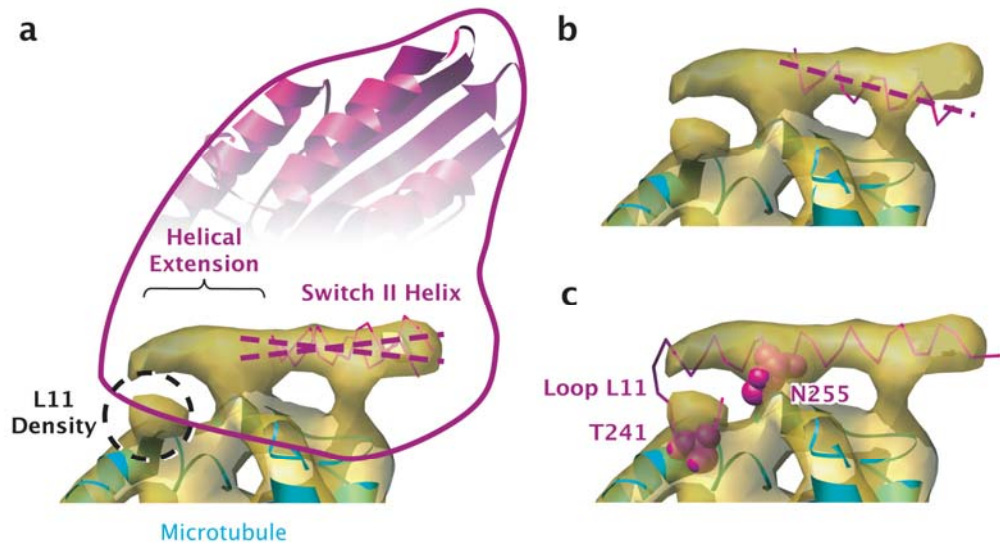
Figure 3

Figure 3. Density for the switch II helix in our cryo-EM map resembles the switch II helix conformation seen in "ADP-like" crystal structures of kinesin, and reveals an N-terminal extension. View orientation is identical to that of Figure 5b. (a) Density map of the switch II helix (see text), with the fitted ADP-like K349 and KIF1A crystal structures superimposed. For clarity, the N-terminal segment of KIF1A's switch II helix, although ordered, was left out of the rendering. The KIF1A structures in (a) and (b) were aligned with our fitted K349 crystal structure by least squares fitting using SwissPDBViewer. The axis of the switch II helix density is intermediate between those of the two crystal structure helices. (b) The axis of the switch II helix from the fitted ATP-like K349 and KIF1A crystal structures does not align with the axis of the helix density. (c) The crystal structure of Kar3 (mutation R598A (Yun et al., 2001)) aligned with the K349 crystal structure coordinates from (a) suggests the architecture of the N-terminal switch II helix extension. The two space-filled residues, T241 and N255, are highly conserved throughout the kinesin family and apparently contact the microtubule surface.
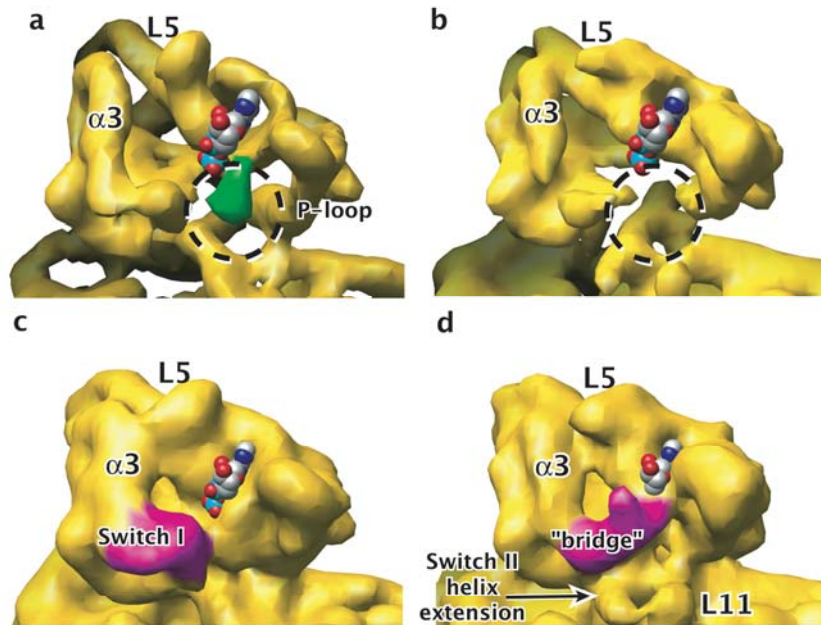
Figure 4

Figure 4. Density map changes in the nucleotide pocket of the nucleotide-free kinesin•microtubule state, relative to the crystallized kinesin•ADP state. The space-filled ADP model indicates the position of the nucleotide pocket. Orientation of the view is approximately the same as in Figure 2b. (a) and (c) show 9Å-resolution synthetic maps, at two different contour levels, generated from the crystal structure of "ADP-like" K349 kinesin (with the ADP coordinates removed). (b) and (d) show our experimental map, at equivalent contour levels to (a) and (c) respectively. In (a), density for the P-loop in the crystal structure is highlighted in green; in (b), the corresponding void in the map is circled. In (c), density corresponding to Switch I is highlighted in magenta; in (d) density corresponding to the "bridge" between Switch I and the nucleotide site is also magenta.
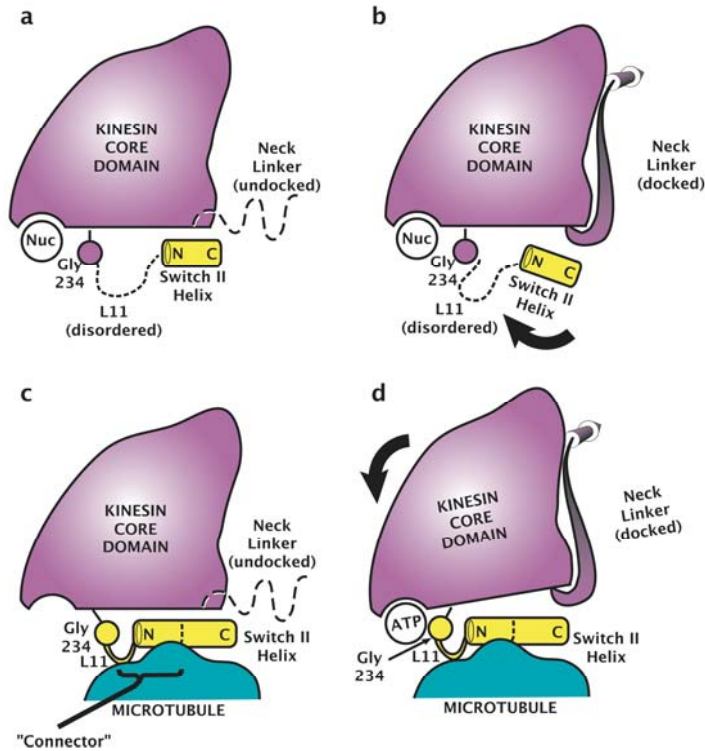
Figure 5

Figure 5. Model for microtubule-induced activation of kinesin's ATP sensing mechanism by partially ordering the L11 segment. The represented view orientation is the same as in Figures 2c and 3. (a)-(b) Coexisting, nucleotide-insensitive conformations of the switch II helix in the absence of the microtubule, modeled after the "ADP-like" (a) and "ATP-like" (b) crystal structures of K349. The presence of various nucleotides in the active site does not trigger any movement of Gly 234, whose position is in any case uncorrelated with that of the switch II helix because L11 is disordered. (c)-(d) Adapted "relay helix" model. In both nucleotide-free (c) and ATP-bound (d) states of kinesin, microtubule contacts order the C-terminal portion of L11 into an extension of the switch II helix plus an additional structured loop. ATP-induced movement of Gly 234 relative to the kinesin core, perhaps "activated" by the closing of switch I (Minehardt et al., 2001), is relayed through the structured L11 assembly (i.e. the "connecter") to the switch II helix, which in turn controls the structure of the neck linker. As previously proposed (Kikkawa et al., 2001), we depict the switch II helix fixed on the surface of the microtubule, so that its movement relative to the kinesin core domain causes the core to move relative to the microtubule surface.